United States Department of Commerce
Technology Administration
National Institute of Standards and Technology

NIST Technical Note 1377

Radiated Emissions and Immunity of Microstrip Transmission Lines: Theory and Measurements

David A. Hill
Dennis G. Camell
Kenneth H. Cavcey
Galen H. Koepke

NIST Technical Note 1377

Radiated Emissions and Immunity of Microstrip Transmission Lines: Theory and Measurements

David A. Hill
Dennis G. Camell
Kenneth H. Cavcey
Galen H. Koepke

Electromagnetic Fields Division
Electronics and Electrical Engineering Laboratory
National Institute of Standards and Technology
325 Broadway
Boulder, Colorado 80303-3328

July 1995

U.S. DEPARTMENT OF COMMERCE, Ronald H. Brown, Secretary
TECHNOLOGY ADMINISTRATION, Mary L. Good, Under Secretary for Technology
NATIONAL INSTITUTE OF STANDARDS AND TECHNOLOGY, Arati Prabhakar, Director

National Institute of Standards and Technology Technical Note
Natl. Inst. Stand. Technol., Tech. Note 1377, 36 pages (July 1994)
CODEN:NTNOEF

U.S. GOVERNMENT PRINTING OFFICE
WASHINGTON: 1994

For sale by the Superintendent of Documents, U.S. Government Printing Office, Washington, DC 20402-9325

CONTENTS

Page

1. INTRODUCTION 1

2. RADIATION FROM MICROSTRIP TRANSMISSION LINES 2
   2.1 Radiation from Horizontal Currents 3
   2.2 Radiation from Vertical Currents 5
   2.3 Total Radiated Power 6
   2.4 Low-Frequency Limit 7
   2.5 Maximum Radiated Field 8

3. REVERBERATION CHAMBER APPROACH 10
   3.1 Radiated Emissions 10
   3.2 Radiated Immunity 11
   3.3 Measured Data 12

4. CONCLUSIONS 15

REFERENCES 15

APPENDIX. RECIPROCITY DERIVATION OF FAR FIELDS 17

RADIATED EMISSIONS AND IMMUNITY OF MICROSTRIP TRANSMISSION LINES: THEORY AND MEASUREMENTS

David A. Hill, Dennis G. Camell, Kenneth H. Cavcey, and Galen H. Koepke

Electromagnetic Fields Division
National Institute of Standards and Technology
Boulder, Colorado 80303

We analyze radiation from a microstrip transmission line and calculate total radiated power by numerical integration. Reverberation chamber methods for measuring radiated emissions and immunity are reviewed and applied to three microstrip configurations. Measurements from 200 to 2000 MHz are compared with theory, and excellent agreement is obtained for two configurations that minimize feed cable and finite ground plane effects. Emissions measurements are found to be more accurate than immunity measurements because the impedance mismatch of the receiving antenna cancels when the ratio of the microstrip and reference radiated power measurements is taken. The use of two different receiving antenna locations for emissions measurements illustrates good field uniformity within the chamber.

Key words: directivity; emissions measurement; immunity measurement; microstrip; mode stirring; radiated power; radiation efficiency; radiation pattern; reverberation chamber; transmission line.

1. INTRODUCTION

The increasing complexity of electronic systems has introduced an increased potential for electromagnetic interference (EMI) between electronic systems [1]. The Federal Communications Commission (FCC) limits on radiated emissions from digital equipment [2] cover the frequency range from 30 to 1000 MHz, and increasing clock rates in digital circuits are likely to result in standards that cover even higher frequencies [3]. The closely related issue of radiated immunity of electronic systems is also receiving increased attention [4,5].

The FCC radiated emission limits specify the maximum radiated electric field measured at a specified distance. In this report we propose an alternative (but related) approach based on the total radiated power over a sphere enclosing the radiating system. The reverberation chamber [6] is a convenient facility for performing total radiated power measurements and radiated immunity measurements [7] over a wide frequency range. It has the advantage of not requiring any rotation of the unknown radiator, but it will not give the directivity or the direction of maximum radiation. To illustrate the theory and measurement procedure, we analyze the simple case of radiation by a single microstrip transmission line [8] and integrate over a far-field sphere to obtain the total radiated power. The reverberation chamber measurement techniques are independent of the actual radiator (or receiver), but we choose the example of a microstrip transmission line because it is an open structure that does radiate and is commonly used in dense circuits and interconnections [9].

The organization of this report is as follows. Section 2 covers the theory of radiation by a microstrip transmission line. A closed-form expression is obtained for the radiation pattern, and a numerical integration is used to obtain the total radiated power. For low frequencies, the numerical integration is performed analytically to obtain an approximate expression for the total radiated power. The directivity of the microstrip is also approximated from its electrical size and compared with the actual directivity. This allows an estimation of the maximum radiated field and hence provides a link to the FCC limit. Section 3 covers the theory for radiated emissions and immunity measurements in a reverberation chamber and includes a comparison of theory and measurements. Section 4 contains conclusions and recommendations for further study. The appendix includes a reciprocity derivation of microstrip, far-field radiation.

2. RADIATION FROM MICROSTRIP TRANSMISSION LINES

The currents on microstrips can be approximated by transmission line theory [10] or determined by a numerical method, such as the method of moments [11]. We choose transmission line theory because of its simplicity, and we also use a line current approximation to compute the radiated field [8]. Both methods typically assume an infinite ground plane and substrate so that the radiated field can be written in terms of the known Sommerfeld integrals or derived by reciprocity [12].

2.1 Radiation from Horizontal Currents

We consider the microstrip geometry shown in figure 1. The x-directed microstrip has length L and width w and is centered at the origin. The substrate has thickness h and permittivity ϵ_s, and the ground plane is located at $z = -h$. The region above the substrate has free-space permittivity ϵ_0, and both regions have free-space permeability μ_0. It is also convenient to define a relative substrate permittivity $\epsilon_{sr} = \epsilon_s/\epsilon_0$. The surface current is approximated by a line current I(x′) located along the x axis. The feed and termination currents are modeled by vertical currents, I(-L/2) and -I(L/2), and their radiation will be considered in the following section.

The field radiated by an infinitesimal horizontal dipole Idx′ can be written in terms of scalar and vector potentials [13] or an electric Hertz vector [8]. Either method results in Sommerfeld integrals [14] which can be evaluated numerically in the near field or by the saddle-point method in the far field [14]. Since we require only far-field expressions, an alternative method is to use reciprocity [12] as described in the appendix.

The θ and ϕ components, $E_{\theta hd}$ and $E_{\phi hd}$, of the electric field radiated by a horizontal dipole can be written in the following forms (see appendix):

$$E_{\theta hd} = \frac{j\omega\mu_0 I dx'}{4\pi} (R_v - 1)\cos\theta\cos\phi \, \frac{e^{-jkR}}{r} \tag{1}$$

and

$$E_{\phi hd} = \frac{j\omega\mu_0 I dx'}{4\pi} (R_h + 1)\sin\phi \, \frac{e^{-jkR}}{r}, \tag{2}$$

where

$$R_v = [1 - \frac{jv}{\epsilon_{sr}\cos\theta} \tan(kvh)]/[1 + \frac{jv}{\epsilon_{sr}\cos\theta} \tan(kvh)], \tag{3}$$

$$R_h = [1 + \frac{jv}{\cos\theta}\cot(kvh)]/[1 - \frac{jv}{\cos\theta}\cot(kvh)], \tag{4}$$

$v = (\epsilon_{sr} - 1)^{1/2}$, $R = r - x'\sin\theta\cos\phi$, $k = \omega(\mu_0\epsilon_0)^{1/2}$, and (r,θ,ϕ) are the standard spherical coordinates. These results are in agreement with the far-field results in [8] obtained by saddle-point evaluation of Sommerfeld integrals. Surface waves are neglected.

To determine the electric field components, $E_{\theta h}$ and $E_{\phi h}$, radiated by the entire horizontal line current, we need to integrate eqs (1) and (2) for $x' = -L/2$ to $L/2$. We assume that the microstrip is fed at $x = -L/2$ and is terminated in a matched load at $x = L/2$. Then the current is a pure traveling wave which we write as

$$I(x') = I_0 \exp(-jk_e x'), \tag{5}$$

where $k_e = k\epsilon_{er}^{1/2}$ and ϵ_{er} is the relative effective dielectric constant for the microstrip mode [15]. Its value lies between ϵ_{sr} and 1. The only x' dependence in eqs (1) and (2) arises from the exponentials. Since the exponentials in eqs (1) and (2) are identical, we have only one integral to evaluate. We can write that integral as an array factor A_L of the type that appears in antenna array theory [16]:

$$A_L = \frac{1}{L}\int_{-L/2}^{L/2} e^{-j(k_e - k\sin\theta\cos\phi)x'} dx' = \frac{\sin[(k_e - k\sin\theta\cos\phi)L/2]}{[(k_e - k\sin\theta\cos\phi)L/2]}. \tag{6}$$

Using eqs (1), (2), and (6), we can write $E_{\theta h}$ and $E_{\phi h}$ as

$$E_{\theta h} = \frac{j\omega\mu_0 I_0 L A_L}{4\pi}(R_v - 1)\cos\theta\cos\phi\,\frac{e^{-jkr}}{r} \tag{7}$$

and

$$E_{\phi h} = \frac{j\omega\mu_0 I_0 L A_L}{4\pi} (R_h + 1)\sin\phi \, \frac{e^{-jkr}}{r}. \tag{8}$$

2.2 Radiation from Vertical Currents

A vertical electric dipole radiates only a θ far-field component $E_{\theta vd}$ which can be written (see appendix):

$$E_{\theta vd} = \frac{j\omega\mu_0 I dz'}{4\pi\epsilon_{sr}} (R_v + 1)\sin\theta \left[\frac{e^{jkv(z'+2h)} + e^{-jkvz'}}{1 + e^{jkv2h}}\right] \frac{e^{-jkR}}{r}. \tag{9}$$

From eq (5), we see that the vertical feed current is $I_0 \exp(jk_e L/2)$ and the vertical termination current is $-I_0 \exp(-jk_e L/2)$. The θ component of the electric field $E_{\theta v}$ is given by the integral of eq (9) over the locations of the feed and termination currents:

$$E_{\theta v} = \int_{z'=-h}^{z'=0} \left(E_{\theta vd}\Big|_{x'=-L/2} - E_{\theta vd}\Big|_{x'=L/2}\right). \tag{10}$$

The differential dz' is contained in $E_{\theta vd}$. By substituting eq (9) into eq (10) and carrying out the z' integration, we obtain

$$E_{\theta v} = \frac{j\omega\mu_0 I_0 F_I}{4\pi\epsilon_{sr} kv} \tan(kvh)(R_v + 1)\sin\theta \, \frac{e^{-jkr}}{r}, \tag{11}$$

where

$$F_I = 2j \sin[(k_e - k\sin\theta\cos\phi)L/2]. \tag{12}$$

2.3 Total Radiated Power

The total radiated θ component is the sum of the radiation by the horizontal and vertical currents: $E_\theta = E_{\theta h} + E_{\theta v}$. Only the horizontal current radiates a ϕ component: $E_\phi = E_{\phi h}$.

We assume that the ground plane and substrate in figure 1 extend to infinity so that the radiated field exists only in the upper half space ($\theta < \pi/2$). We can write the total radiated power P_r as an integral over a hemisphere at large r:

$$P_r = r^2 \int_0^{2\pi} \int_0^{\pi/2} \frac{(|E_\theta|^2 + |E_\phi|^2)}{\eta} \sin\theta \, d\theta d\phi, \tag{13}$$

where $\eta = (\mu_0/\epsilon_0)^{1/2}$. Generally the double integration in eq (13) needs to be performed numerically, but in the following section we perform the integration analytically for the low-frequency limit.

For the usual case of weak radiation, most of the input power P_i to the microstrip is dissipated in the matched load. Thus we can approximate P_i by

$$P_i = |I_0|^2 Z_0, \tag{14}$$

where Z_0 is the characteristic impedance [15] of the microstrip. Thus we can approximate the radiation efficiency Eff by

$$\mathrm{Eff} = P_r/P_i = \frac{P_r}{|I_0|^2 Z_0}. \tag{15}$$

If the detailed expression for P_r is substituted into eq (15), the denominator $|I_0|^2$ cancels out.

2.4 Low-Frequency Limit

In the low-frequency limit, we assume that the quantities, kh, kL, and $k_e L$, are small. Consequently we make the following small argument approximations:

$$A_L \approx 1, \tag{16}$$

$$F_I \approx j(k_e - k\sin\theta\cos\phi)L, \tag{17}$$

$$\cot(kvh) \approx (kvh)^{-1}, \tag{18}$$

and

$$\tan(kvh) \approx kvh. \tag{19}$$

If we use the approximations in eqs (16) through (19) and retain only the leading term in k^2Lh, we can write the squares of the electric field components as

$$|E_\theta|^2 \approx \frac{(I_0 k^2 Lh\eta)^2}{(2\pi r)^2}\left(\cos^2\phi - 2\frac{\epsilon_{er}^{1/2}}{\epsilon_{sr}}\sin\theta\cos\phi + \frac{\epsilon_{er}}{\epsilon_{sr}^2}\sin^2\theta\right) \tag{20}$$

and

$$|E_\phi|^2 \approx \frac{(I_0 k^2 Lh\eta)^2}{(2\pi r)^2}\cos^2\theta\sin^2\phi. \tag{21}$$

If we substitute eqs (20) and (21) into eq (13), we can perform the θ and ϕ integrations analytically with the following result:

$$P_r \approx \frac{I_0^2\eta(k^2Lh)^2}{3\pi}\left(1 + \frac{\epsilon_{er}}{\epsilon_{sr}^2}\right). \tag{22}$$

If we had assumed a constant current $I(x') = I_0$ on the microstrip in eq (5), then we would have obtained the result in eq (22) with $\epsilon_{er} = 0$:

$$P_r\Big|_{\epsilon_{er}=0} \approx \frac{I_0^2\eta(k^2Lh)^2}{3\pi}. \tag{23}$$

The result in eq (23) agrees with the power radiated by a vertical half loop of area Lh carrying a constant current I_0 over a perfectly conducting plane in free space [16]. The result for the traveling-wave current in eq (22) is larger, but both eqs (22) and (23) have the expected $k^4 \cdot \text{area}^2$ dependence which is characteristic of an electrically small loop.

2.5 Maximum Radiated Field

In order to relate total radiated power to the maximum radiated electric field (as specified in the FCC regulations), we need to know the directivity D of the radiator. The maximum radiated electric field E_{max} at a distance r is

$$E_{max} = \frac{1}{r}\left(\frac{\eta D P_r}{4\pi}\right)^{1/2}. \tag{24}$$

Normally the directivity of an inadvertant radiator, such as a microstrip transmission line, is not known. However, if we exclude the unlikely possibility of supergain, the maximum directivity of a radiator is determined by its electrical size [17,18]. For a radiator that can be enclosed within a sphere of radius a, the maximum directivity D_m is

$$D_m = \begin{cases} 3, & ka \le 1 \\ (ka)^2 + 2ka, & ka > 1. \end{cases} \tag{25}$$

The case of $ka < 1$ corresponds to combined electric and magnetic dipole radiation in the form of a Huygens source [18], and the case of $ka > 1$ corresponds to general spherical multipole radiation.

For our microstrip geometry, we can set $a = L/2$. However, we must also account for the effect of the infinite ground plane. By image theory considerations, we can show that the maximum directivity of a source over a ground plane can be twice that of the same source in free space. Consequently, we can write the maximum directivity of the microstrip as

$$D_m = \begin{cases} 6, & kL/2 \le 1 \\ 2(kL/2)^2 + kL, & kL/2 > 1. \end{cases} \tag{26}$$

To illustrate the frequency dependence of the directivity, we consider an example with the following parameters: $h = 1.55$ mm, $L = 10$ cm, $w = 4.8$ mm, and $\epsilon_{sr} = 2.2$. These parameters yield a characteristic impedance $Z_0 = 50\ \Omega$ and an effective permittivity $\epsilon_{er} = 1.881$ [15]. In figure 2 we show the maximum directivity determined from eq (26) and the actual directivity determined by numerically evaluating the radiated power in eq (13). Both quantities increase with frequency, but the actual directivity is always less than the maximum directivity. Consequently, eq (24) yields an upper bound for the maximum radiated electric field.

The direction of maximum radiation is also of some interest. Our program for directivity also computes the direction of maximum radiation. For our simple microstrip geometry, the maximum radiation always occurs at zero or 180° azimuth. Figure 3 shows a plot of the zenith angle θ of maximum radiation for the same parameters as considered in figure 2. In order to plot zenith angle continuously, we allow θ to range from -90° to 90°. As the frequency increases, the array factor A in eq (8) forces the radiation from the back direction toward 90° like an end-fire, traveling-wave antenna.

3. REVERBERATION CHAMBER APPROACH

Although we computed the total radiated power by integrating the power density over a large hemisphere as indicated by eq (13), we prefer not to require radiated field measurements over a surface enclosing the radiator. The reverberation chamber [6] is a convenient facility for measuring total radiated power without requiring motion of the receiving antenna or the radiator. It is equally convenient for performing radiated immunity measurements [7].

3.1 Radiated Emissions

Consider the reverberation chamber (cavity) geometry shown in figure 4. In our measurements the radiator was a microstrip transmission line, but the theory and measurement method apply to any radiator. A mode stirrer (tuner) is used to obtain uniform power density throughout the chamber, and this technique requires that the cavity be electrically large (so that the cavity is multimoded).

A power conservation approach [19,20] shows that the power density S_c in the chamber is

$$S_c = \frac{\lambda Q P_r}{2\pi V}, \tag{27}$$

where λ is the free-space wavelength, V is the cavity volume, Q is the cavity quality factor, and P_r is the radiated power. Strictly speaking, S_c in eq (27) and received power in equations to follow are ensemble averages over all stirrer positions. The chamber Q is normally measured by a transmission loss method [6,17] or a pulse decay method [21], but it can calculated if all the loss mechanisms are known [20].

In a reverberation chamber, the effective area of a lossless, impedance-matched receiving antenna is $\lambda^2/8\pi$ [19,20]. The received power P_{rec} is then given by the product of the power density and the effective area:

$$P_{rec} = S_c \frac{\lambda^2}{8\pi} = \frac{\lambda^3 Q}{16\pi^2 V} P_r. \tag{28}$$

If we measure the received power, eq (28) can be used to measure the radiated power. If we also measure the input power P_i, then we can determine the radiation efficiency from eqs (15) and (28):

$$\text{Eff} = P_r/P_i = \frac{16\pi^2 V P_{rec}}{\lambda^2 Q P_i}. \tag{29}$$

3.2 Radiated Immunity

Typically both a receiving (reference) antenna and a transmitting antenna are used for radiated immunity measurements as shown in figure 4. The power received by the reference antenna is P_{ref}, and the power received by the microstrip is P_{rm}. We define the shielding effectiveness (SE) in decibels in terms of the received power ratio [7]:

$$SE = 10 \log_{10}(P_{ref}/P_{rm}), \text{ dB}. \tag{30}$$

With the above definition, SE is normally positive.

Another valid descriptor of the receiving properties of the microstrip is the effective area A_e [7]. The effective area can be determined from the received power as follows:

$$A_e = \frac{P_{rm}}{S_c} = \frac{P_{rm}}{P_{ref}} \frac{\lambda^2}{8\pi}. \tag{31}$$

From eqs (30) and (31), we can also write SE in terms of A_e:

$$SE = 10 \log_{10}[\lambda^2/(8\pi A_e)], \text{ dB}. \tag{32}$$

By reciprocity [12], we can show that the effective area of the microstrip is simply related to the radiation efficiency:

$$A_e = \text{Eff} \frac{\lambda^2}{8\pi}. \tag{33}$$

From eqs (31) and (33), we can also write radiation efficiency as

$$\text{Eff} = \frac{8\pi A_e}{\lambda^2} = \frac{P_{rm}}{P_{ref}}. \tag{34}$$

For the emissions measurement, we can interpret P_{rm} as the power measured by the reference antenna when the microstrip is transmitting and P_{ref} as the power measured by the reference antenna when the other antenna is transmitting. Equation (34) is actually preferred to eq (29) for measuring the radiation efficiency because the chamber Q is needed for use of eq (29). Equations (29) and (34) are mathematically equivalent when the usual expression for chamber Q [19,20] is substituted into eq (29).

Equation (33) indicates that both the emissions and immunity properties of the microstrip could in theory be obtained from either emissions or immunity measurements. However, considering the relatively large uncertainty of reverberation chamber measurements [6], it is useful to do both emissions and immunity measurements and to use eq (33) as a consistency (reciprocity) check.

3.3 Measured Data

In order to study feed and mounting effects, we constructed two microstrip transmission line boards with the same microstrip parameters, but different ground plane dimensions and feeds. The microstrip transmission line parameters ($h = 1.55$ mm, $L = 10$ cm, $w = 4.8$ mm, and $\epsilon = 2.2$) are the same as those used for the pattern calculations in Section 2.5. The first board is 10 cm by 10 cm with a coaxial feed line oriented as shown in figure 5. This board can be tested in the conventional raised position away from all chamber walls, or it can be bonded to the chamber floor to achieve an extended ground plane and to short circuit currents on the exterior of the coaxial feed. The second larger board (23 cm by 30 cm) has the microstrip line centered with the coaxial feed line and the termination located below the board as shown in figure 6. This board is a closer approximation to the theoretical model because the ground plane is larger and the coaxial feed line is fairly well shielded by the ground plane.

Figure 7 shows a comparison of theory and measurements for radiated emissions from 200 to 2000 MHz. The lower frequency limit of 200 MHz is determined by the need for a sufficient mode density in the NIST reverberation chamber [6]. The chamber mode density increases with frequency, but the approximate microstrip theory in Section 2 is not valid above 2000 MHz. The results are given as the power ratio (in decibels) for the reference antenna transmitting compared to the microstrip transmitting, but the results could be converted to radiation efficiency by using eq (34). One advantage of presenting the results as a power ratio is that the emissions results can be directly compared with the immunity results for SE. The theoretical curve is smooth, but the measured curves show modal oscillations that are characteristic of reverberation chamber data [6]. Log-periodic dipole antennas were used for the transmitting and receiving antennas below 1000 MHz, and broadband ridged horns were used above 1000 MHz. The power radiated by the reference antenna is the incident minus reflected power. Thus impedance mismatch loss is taken into account for the reference transmitting antenna, but not for the receiving antenna. The measurement data were generated by averaging received power over 200 stirrer positions at each frequency.

At low frequencies (small kL), the k^4 dependence of the radiated power in eq (23) indicates that the slope in figure 7 should be approximately -12 dB/octave, and this behavior holds below 500 MHz. The measurements for the raised microstrip with the end feed (as shown in figure 5 show the poorest agreement with theory, probably because of radiation from the shield of the coaxial line and edge effects of the small ground plane. The measurements for the bottom feed show the best agreement with theory, but the measurements for the bonded microstrip also show good agreement with theory. This indicates that test objects that operate with a ground plane can be conveniently mounted on chamber walls even though conventional practice has normally placed test objects at least a wavelength from chamber walls. The plane wave spectrum theory for fields in reverberation chambers [7,22] indicates that wall mounting is appropriate for ground plane test objects, and wall mounting also provides a convenient means for short circuiting the shields of feed cables.

Figure 8 shows the analogous comparison of measurements and theory for the radiated immunity case. These results can be considered to represent SE in decibels. These measurements can be performed more quickly than emissions measurements because the power received by the reference antenna and the microstrip are measured simultaneously. However, the measurements are not as accurate because the impedance mismatch of the reference receiving antenna is not taken into account. (In emissions measurements, the impedance mismatch of the receiving antenna approximately cancels when the ratio for the reference antenna and microstrip transmitting is taken.) However, the agreement is still satisfactory for the bottom feed and bonded microstrip cases.

As indicated by eq (28), we assume that the effective area of the reference antenna is $\lambda^2/8\pi$. In figures 7 and 8, the crossover frequency of 1000 MHz actually includes two points, representing the log-periodic dipole antenna and the ridged horn antenna. The small difference (approximately 1 dB) between these two points is a good confirmation that the specific antenna and antenna pattern are unimportant in reverberation chamber measurements. Another assumption in reverberation chamber measurements is field uniformity throughout the chamber. For emissions measurements, we measured power received by each antenna when the microstrip was transmitting. The two antennas (log periodics or horns) were placed on opposite sides of the chamber and thus provide a field uniformity check. Figures 9 through 11 show the emissions measurements for the two different receiving antennas, and the measured difference is typically on the order of 1 dB except at the lower frequencies. These results are consistent with earlier field uniformity measurements [6].

4. CONCLUSIONS

We have derived closed-form expressions for the fields radiated by a microstrip transmission line and have calculated total radiated power by numerical integration. For low frequencies, we have obtained an approximate expression for the total radiated power that is similar to the expression for radiation by a small loop. We have also approximated the directivity of the loop in order to provide a link to FCC limits on radiated electric field. We have reviewed the theory for radiated emissions and immunity measurements in reverberation chambers and shown how they are related. A comparison of theory and measurements for both emissions and immunity from 200 to 2000 MHz shows excellent agreement for the two microstrip geometries (bottom feed and bonded to chamber floor) that minimize feed cable effects. The emissions measurements show somewhat better agreement with theory than the immunity measurements because the impedance mismatch of the receiving antenna cancels when the ratio with the reference measurement is taken. Field uniformity was demonstrated to be good by measuring the microstrip radiation in two different chamber locations.

A number of extensions to this work would be worthwhile. Emissions and immunity calculations could be performed for more complex circuit boards with complex wire connections [23] and finite ground planes [24]. The reverberation chamber measurement technique described here is valid for general test objects and higher frequencies that will continue to become more important. Time-domain analysis [4] and measurements should be pursued because of the importance of digital systems. Some pulsed measurements have been performed in reverberation chambers [25] and other cavities [26], but further study of pulsed measurements in reverberation chambers is needed. Also, frequency stirring [27,28] should be employed on immunity measurements for increased speed and possibly increased accuracy.

REFERENCES

[1] Paul, C.R. Modeling electromagnetic interference properties of printed circuit boards. IBM J. Res. Dev., 33: 33-50; 1989.

[2] Keenan, R.K. Digital Design for Interference Specifications. Pinellas Park, FL: Kennan Corp.; 1983.

[3] Gravelle, L.B.; Wilson, P.F. EMI/EMC in printed circuit boards -- a literature review. IEEE Trans. Electromag. Compat., 34: 109-116; 1992.

[4] Bernardi, P.; Cicchetti, R.; Pirone, C. Transient response of a microstrip line circuit excited by an external electromagnetic source. IEEE Trans. Electromag. Compat., 34: 100-108; 1992.

[5] Sali, S. Coupling of antenna fields to planar microstrip transmission lines. IEE Conf. Anten. Propagat.: 41-44; 1993.

[6] Crawford, M.L.; Koepke, G.H. Design, evaluation, and use of a reverberation chamber for performing electromagnetic susceptibility/vulnerability measurements. Nat. Bur. Stand. (U.S.) Tech. Note 1092; 1986.

[7] Hill, D.A.; Crawford, M.L.; Kanda, M.; Wu, D.I. Aperture coupling to a coaxial air line; theory and experment. IEEE Trans. Electromag. Compat., 35: 69-74; 1993.

[8] Costa, M.; Sarkar, T.K.; Strait, B.J. On radiation from printed circuits. IEEE Int. Symposium Electromag. Compat.: 246-249; 1981.

[9] Goldfarb, M.; Platzker, A. The effects of electromagnetic coupling on MMIC design. Int. J. Microwave Millimeter Wave CAE, 1: 38-47; 1991.

[10] Daijavad, S.; Janak, J.; Heeb, H.; Ruehli, A.; McBride, D. A fast method for computing radiation from printed circuit boards. IEEE Int. Symposium Electromag. Compat.: 300-304; 1990.

[11] Aksun, M.I.; Mittra, R. Spurious radiation from microstrip interconnects. IEEE Trans. Electromag. Compat., 35: 148-158; 1993.

[12] Monteath, G.D. Applications of the Electromagnetic Reciprocity Principle. Oxford: Pergamon Press; 1973.

[13] Gardiol, F.E. Radiation from microstrip circuits: an introduction. Int. J. Microwave Millimeter Wave CAE, 1: 225-235; 1991.

[14] Banos, A. Dipole radiation in the presence of a conducting half-space. New York: Pergamon Press; 1966, Ch. 3, On the saddle-point method of integration.

[15] Hoffman, R.K. Handbook of Microwave Integrated Circuits. Norwood, MA: Artech House; 1987.

[16] Harrington, R.F. Time-Harmonic Electromagnetic Fields. New York: McGraw-Hill; 1961.

[17] Harrington, R.F. Effect of antenna size on gain, bandwidth, and efficiency. J. Res. Nat. Bur. Stand. (U.S.), 64D: 1-12; 1960.

[18] Hansen, J.E. Spherical Near-Field Antenna Measurements. London: Peter Peregrinus; 1988, Sec. 2.4.4.

[19] Corona, P.; Latmiral, G.; Paolini, E. Performance and analysis of a reverberating enclosure with variable geometry. IEEE Trans. Electromag. Compat., EMC-22: 2-5; 1980.

[20] Hill, D.A.; Adams, J.W.; Ma, M.T.; Ondrejka, A.R.; Riddle, B.F.; Crawford, M.L.; Johnk, R.T. Aperture excitation of electrically large, lossy cavities. Natl. Inst. Stand. Technol. Tech. Note 1361; 1993.

[21] Richardson, R.E. Mode-stirred chamber calibration factor, relaxation time, and scaling laws. IEEE Trans. Instrum. Meas., IM-34: 573-580; 1985.

[22] Dunn, J.M. Local, high-frequency analysis of the fields in a mode-stirred chamber, IEEE Trans. Electromag. Compat., 32: 53-58; 1990.

[23] Hill, R.L.; Van Doren, T.; Hubing, T.; Drewniak, J. Common mode currents induced on wires attached to multilayer printed wire boards with segmented ground planes. IEEE Int. Symposium Electromag. Compat.: 116-120; 1994.

[24] Daijavad, S.; Pence, W.; Heeb, H.; Ponnapalli, S.; Ruehli, A. Methodology for eveluating practical EMI design guidelines using EM analysis programs. IEEE Int. Symposium Electromag. Compat.: 30-34; 1992.

[25] Crawford, M.L.; Ma, M.T.; Ladbury, J.M.; Riddle, B.F. Measurement and evaluation of a TEM/reverberating chamber. Natl. Inst. Stand. Technol. Tech. Note 1342; 1990.

[26] Hill, D.A.; Crawford, M.L.; Johnk, R.T.; Ondrejka, A.R.; Camell, D.G. Measurements of shielding effectiveness and cavity characteristics of airplanes. Natl. Inst. Stand. Technol. NISTIR 5023; 1994.

[27] Loughry, T.A. Frequency stirring: an alternate approach to mechanical mode-stirring for the conduct of electromagnetic susceptibility testing. Phillips Laboratory, PL-TR--91-1036; 1991.

[28] Hill, D.A. Electronic mode stirring for reverberation chambers. IEEE Trans. Electromag. Compat., 36: 294-299; 294.

APPENDIX. RECIPROCITY DERIVATION OF FAR FIELDS

A reciprocity derivation [12] of the far fields can be obtained by locating a test source at a large distance from the origin and calculating the horizontal electric field at the air-substrate interface and the vertical electric field within the substrate. The geometry is the same as in figure 1, except that the source is now a distant electric dipole source that radiates a plane wave in the vicinity of the origin. The elevation incidence angle is θ, and for simplicity we set the azimuthal incidence angle ϕ equal to 0.

Consider first the horizontal polarization case. The total electric field E_{y0} in free space ($z > 0$) can be written

$$E_{y0} = E_0\, e^{jkx\sin\theta} \left(e^{jkz\cos\theta} + R_h e^{-jkz\cos\theta}\right), \tag{A1}$$

where

$$E_0 = \frac{-j\omega\mu_0 I d\ell}{4\pi} \frac{e^{-jkr_d}}{r_d}, \tag{A2}$$

$d\ell$ is the dipole moment, and r_d is the dipole distance from the origin. The magnetic field has both x and z components. The magnetic field x component H_{x0} in free space is

$$H_{x0} = \frac{E_0 \cos\theta}{\eta}\, e^{jkx\sin\theta} \left(e^{jkz\cos\theta} - R_h e^{-jkz\cos\theta}\right). \tag{A3}$$

Within the substrate ($-h < z < 0$), the electric field E_{ys} can be written

$$E_{ys} = E_0\, e^{jkx\sin\theta} \left(Ae^{jkvz} + Be^{-jkvz}\right), \tag{A4}$$

where A is the unknown coefficient of the downgoing wave and B is the unknown coefficient of the upgoing wave. From Maxwell's curl equation, we can write the x component of the magnetic field H_{xs} in the substrate as

$$H_{xs} = \frac{E_0 v}{\eta}\, e^{jkx\sin\theta} \left(Ae^{jkvz} - Be^{-jkvz}\right). \tag{A5}$$

The boundary conditions are that the tangential components of the electric and magnetic fields are continuous at the air-substrate interface and that the tangential electric field is zero at the ground plane:

$$(E_{y0} - E_{ys})\big|_{z=0} = 0, \tag{A6}$$

$$(H_{x0} - H_{xs})\big|_{z=0} = 0, \tag{A7}$$

and

$$E_{ys}\big|_{z=-h} = 0. \tag{A8}$$

Simultaneous solution of eqs (A6) through (A8) yields expressions for A, B, and R_h. A and B are not needed to determine the electric field at the interface, and the expression for R_h is that given in eq (4).

The tangential electric field at the air-substrate interface is

$$E_{y0}\big|_{z=0} = E_0(R_h + 1)\, e^{jkx\sin\theta}. \tag{A9}$$

If we generalize eq (A9) to allow arbitrary azimuthal incidence angle, we obtain the reciprocal result for horizontal dipole radiation in eq (2).

We now consider vertical polarization where the source is a θ-oriented electric dipole. The total magnetic field H_{y0} in free space can be written

$$H_{y0} = \frac{-E_0}{\eta}\, e^{jkx\sin\theta}\, (e^{jkz\cos\theta} + R_v e^{-jkz\cos\theta}). \tag{A10}$$

The electric field has both x and z components. The electric field component E_{x0} in free space is

$$E_{x0} = E_0\cos\theta\, e^{jkx\sin\theta}\, (e^{jkz\cos\theta} - R_v e^{-jkz\cos\theta}). \tag{A11}$$

Within the substrate, the magnetic field H_{ys} can be written

$$H_{ys} = \frac{-E_0}{\eta} e^{jkx\sin\theta} (Ce^{jkvz} + De^{-jkvz}), \tag{A12}$$

where C is the unknown coefficient of the downgoing wave and D is the unknown coefficient of the upgoing wave. From Maxwell's curl equation, we can write the x component E_{xs} and z component E_{zs} of the electric field in the substrate as

$$E_{xs} = \frac{vE_0}{\epsilon_{sr}} e^{jkx\sin\theta} (Ce^{jkvz} - De^{-jkvz}) \tag{A13}$$

and

$$E_{zs} = \frac{-E_0\sin\theta}{\epsilon_{sr}} e^{jkx\sin\theta} (Ce^{jkvz} + De^{-jkvz}). \tag{A14}$$

The boundary conditions are again that the tangential components of the electric and magnetic field are continuous at the air-substrate interface and that the tangential electric field is 0 at the ground plane:

$$(H_{y0} - H_{ys})\big|_{z=0} = 0, \tag{A15}$$

$$(E_{x0} - E_{xs})\big|_{z=0} = 0, \tag{A16}$$

and

$$E_{xs}\big|_{z=-h} = 0. \tag{A17}$$

Simultaneous solution for eqs (A15) through (A17) yields the result for R_v given in eq (3) and the following expressions for D and C:

$$D = (1 + R_v)/(1 + e^{j2kvh}) \tag{A18}$$

and

$$C = De^{j2kvh}. \tag{A19}$$

The tangential electric field at the air-substrate interface is

$$E_{x0}\Big|_{z=0} = E_0(1 - R_v)\cos\theta \; e^{jkx\sin\theta} \tag{A20}$$

If we generalize eq (A20) to allow for arbitrary azimuthal incidence angle, we obtain the reciprocal result for horizontal dipole radiation in eq (1).

The vertical electric field E_{zs} within the substrate is given by eq (A14) where C and D are given by eqs (A18) and (A19). This result is independent of azimuthal incidence angle. So the reciprocal result for vertical dipole radiation in eq (9) is obtained directly from eq (A14).

Other electric and magnetic dipole source results could be obtained easily by this reciprocity method, but they are not shown here because they are not required for computing microstrip radiation.

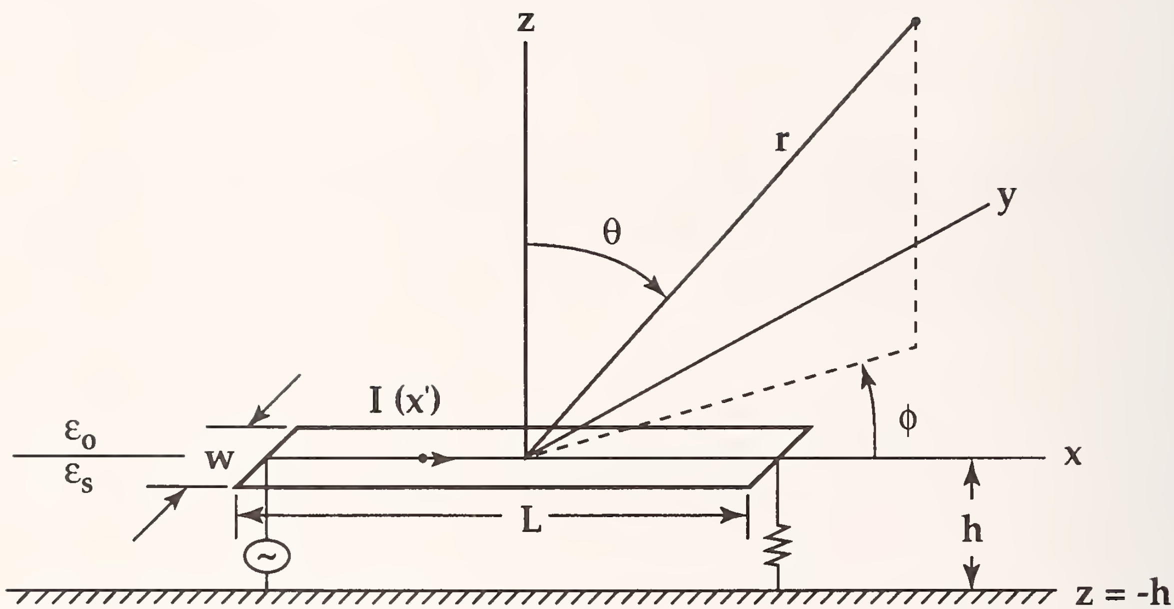

Figure 1. Geometry for a microstrip transmission line of length L.

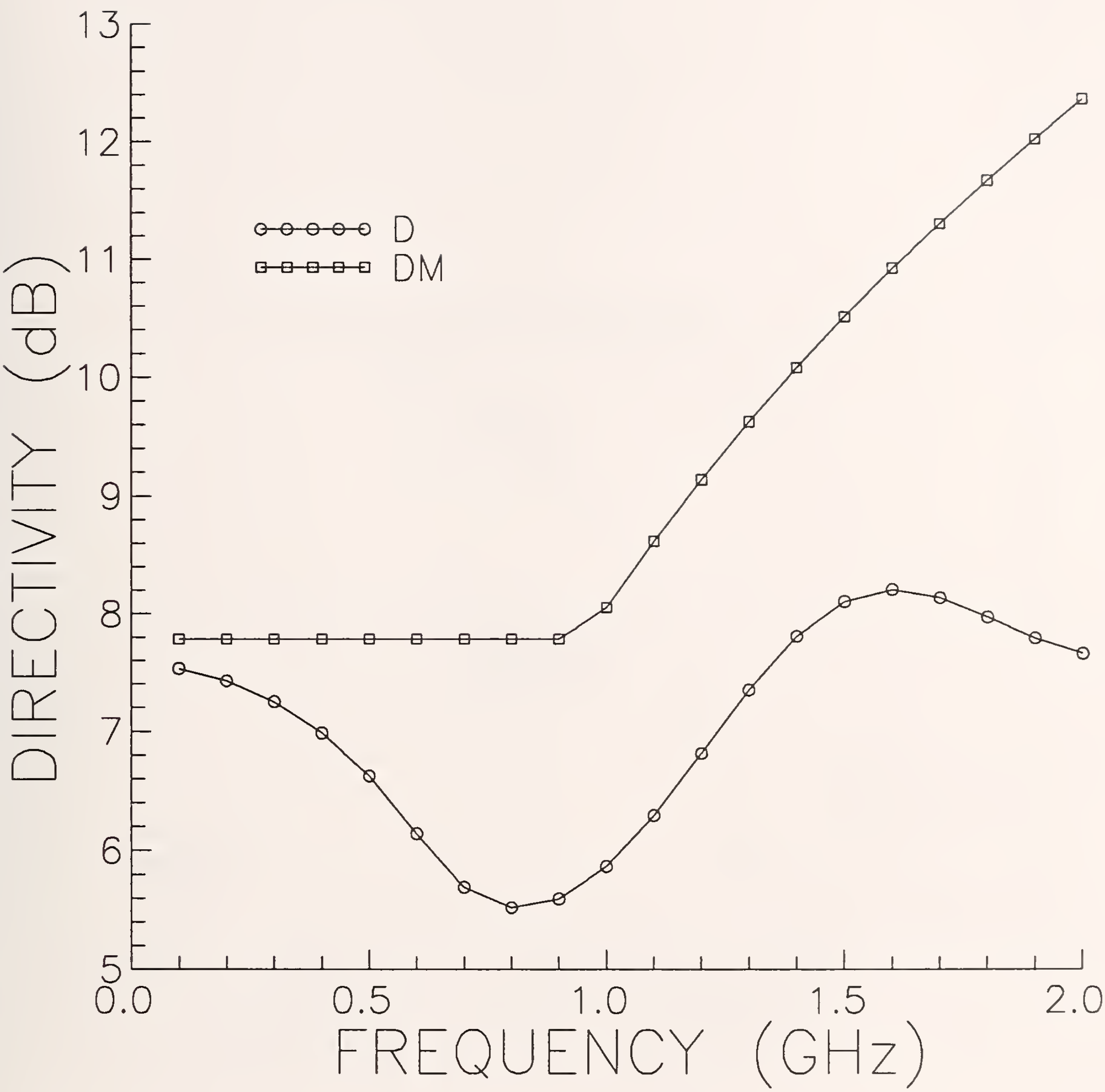

Figure 2. Maximum (DM) and actual (D) directivity of microstrip line. Parameters: L = 10 cm, w = 4.8 mm, h = 1.55 mm, and ϵ_{sr} = 2.2.

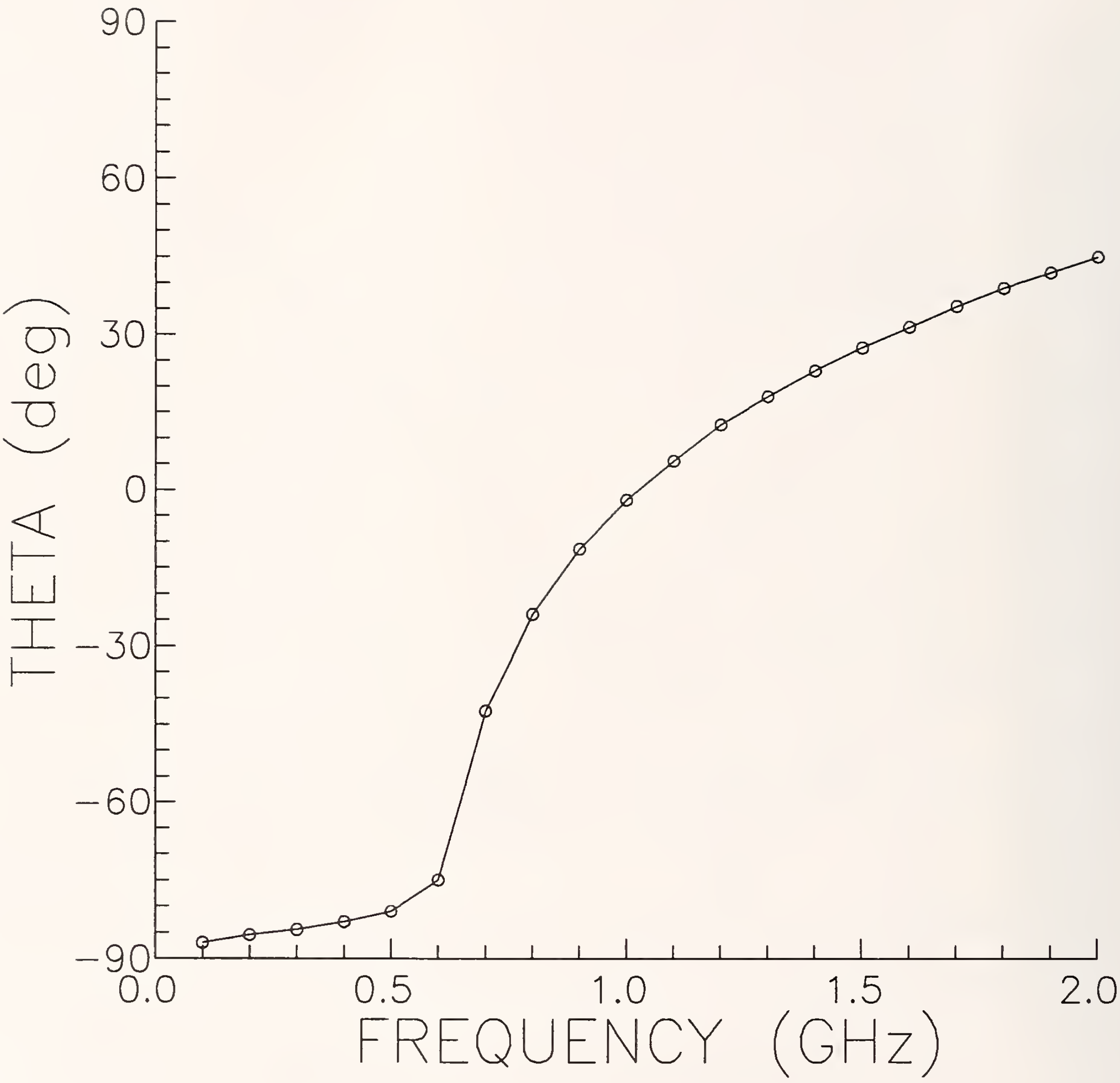

Figure 3. Angle of maximum radiation of microstrip line. Parameters: L = 10 cm, w = 4.8 mm, h = 1.55 mm, and ϵ_{sr} = 2.2.

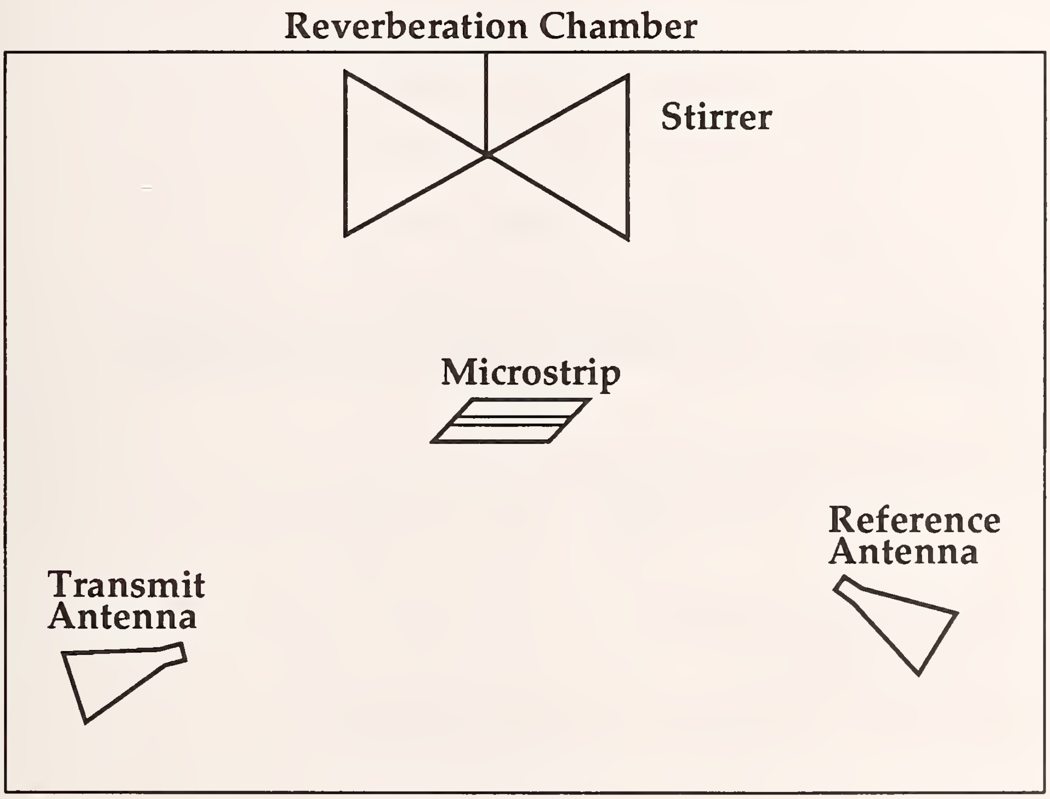

Figure 4. Reverberation chamber configuration for emissions or immunity measurements.

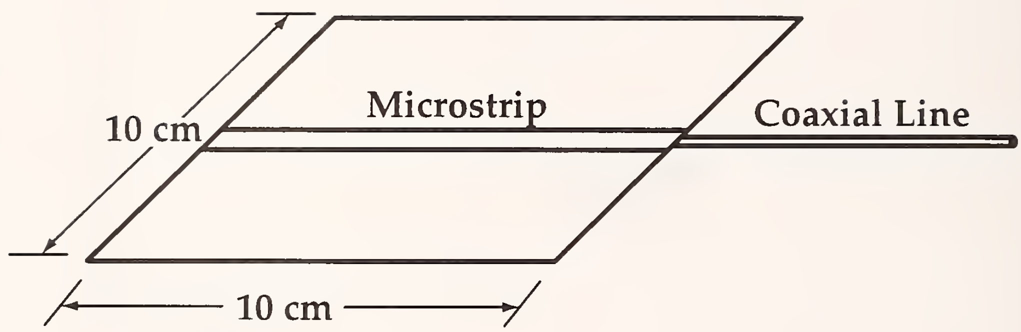

Figure 5. Microstrip transmission line with end feed.

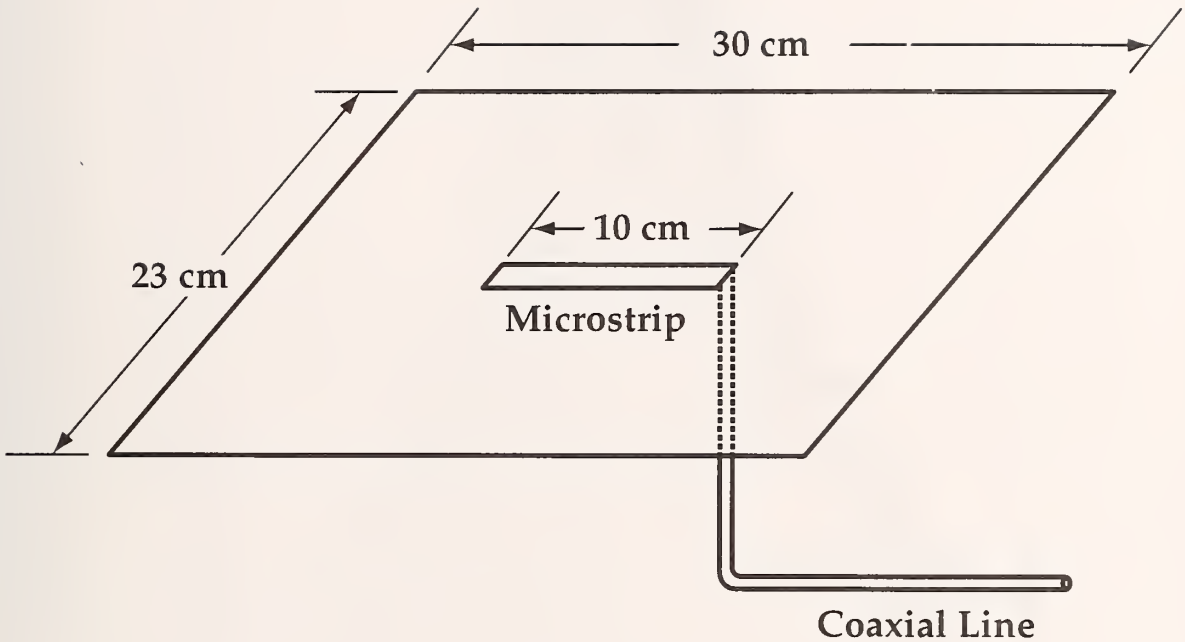

Figure 6. Microstrip transmission line with bottom feed.

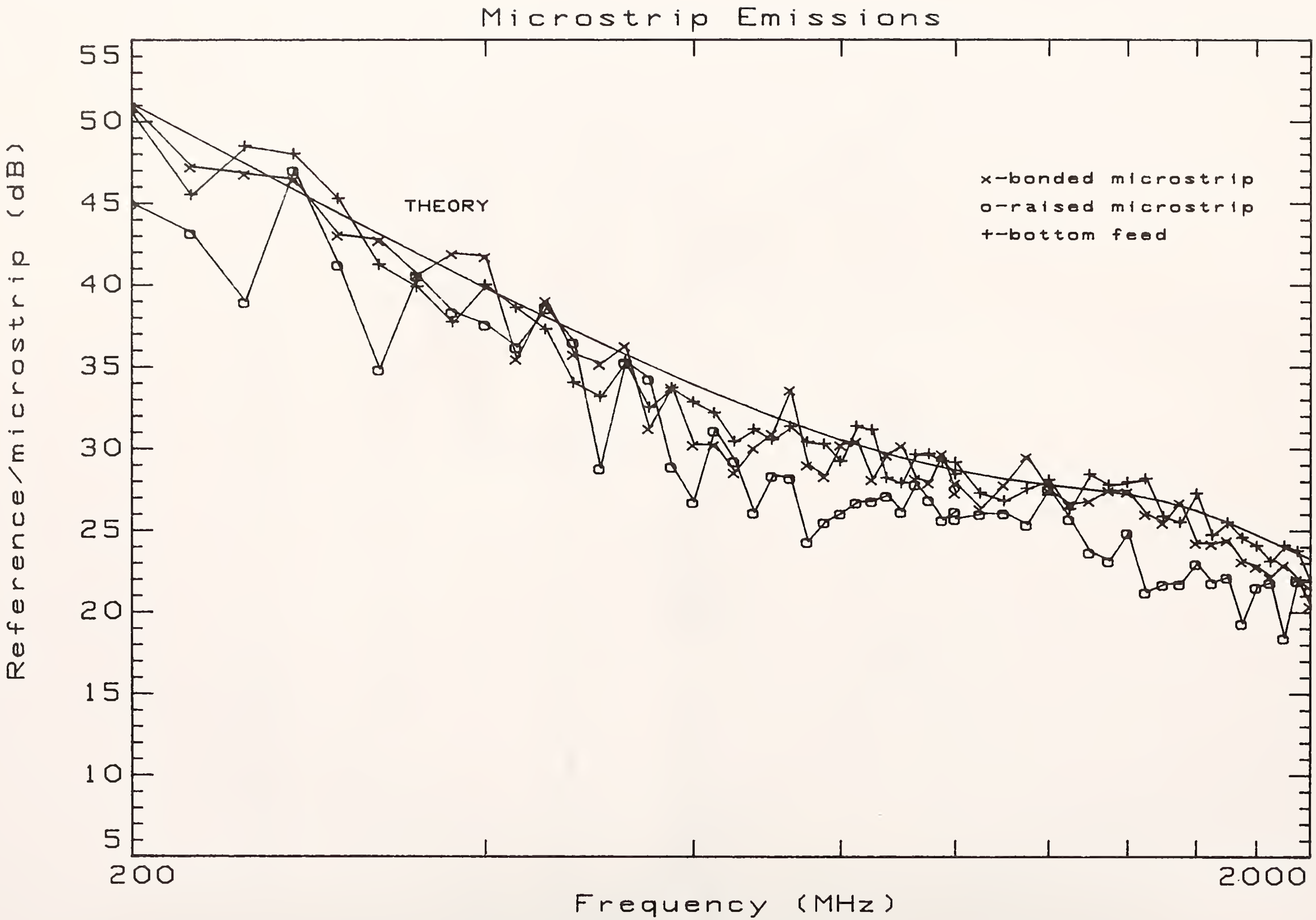

Figure 7. Theory (smooth curve) and measurements for microstrip emissions.

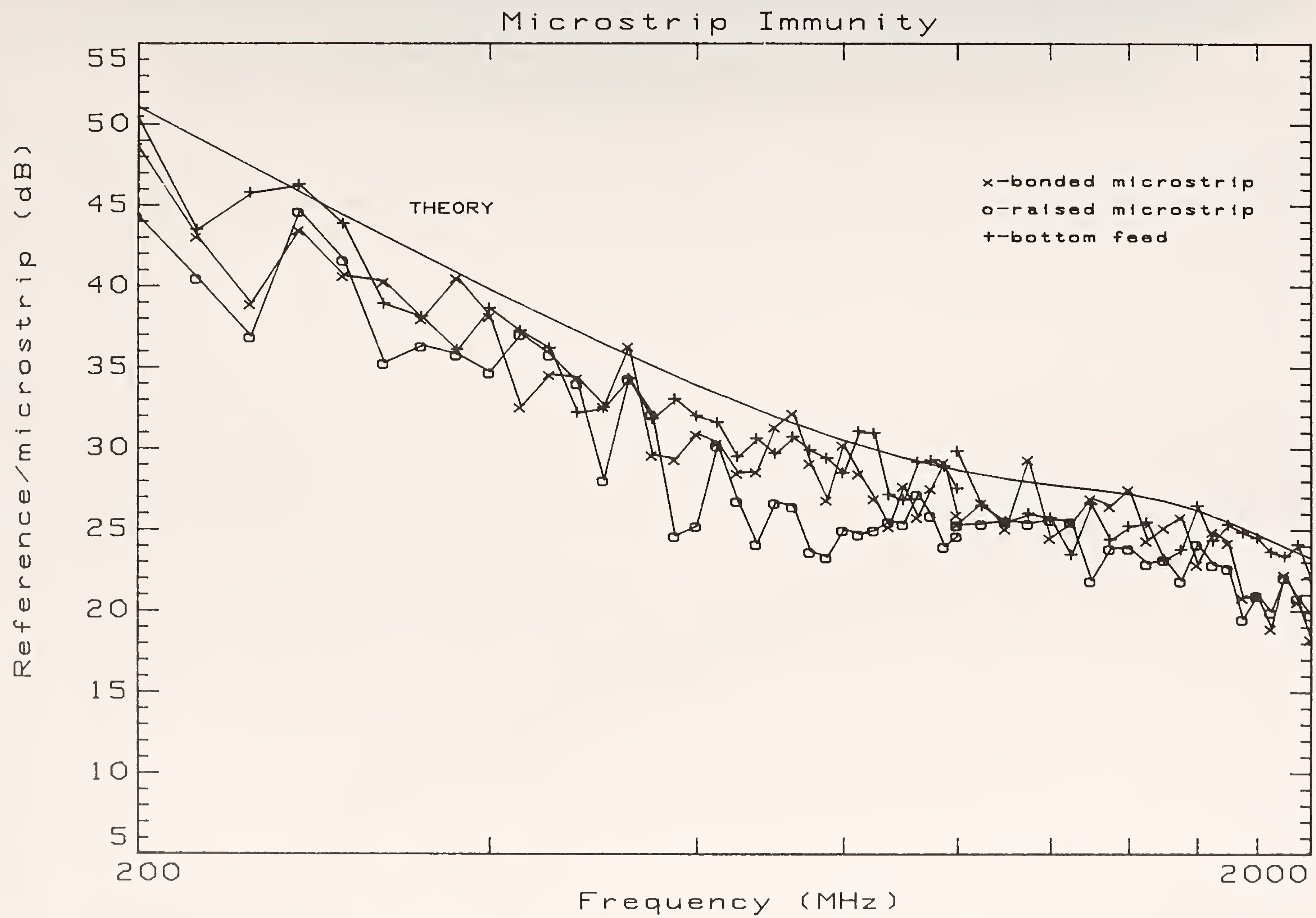

Figure 8. Theory (smooth curve) and measurements for microstrip immunity.

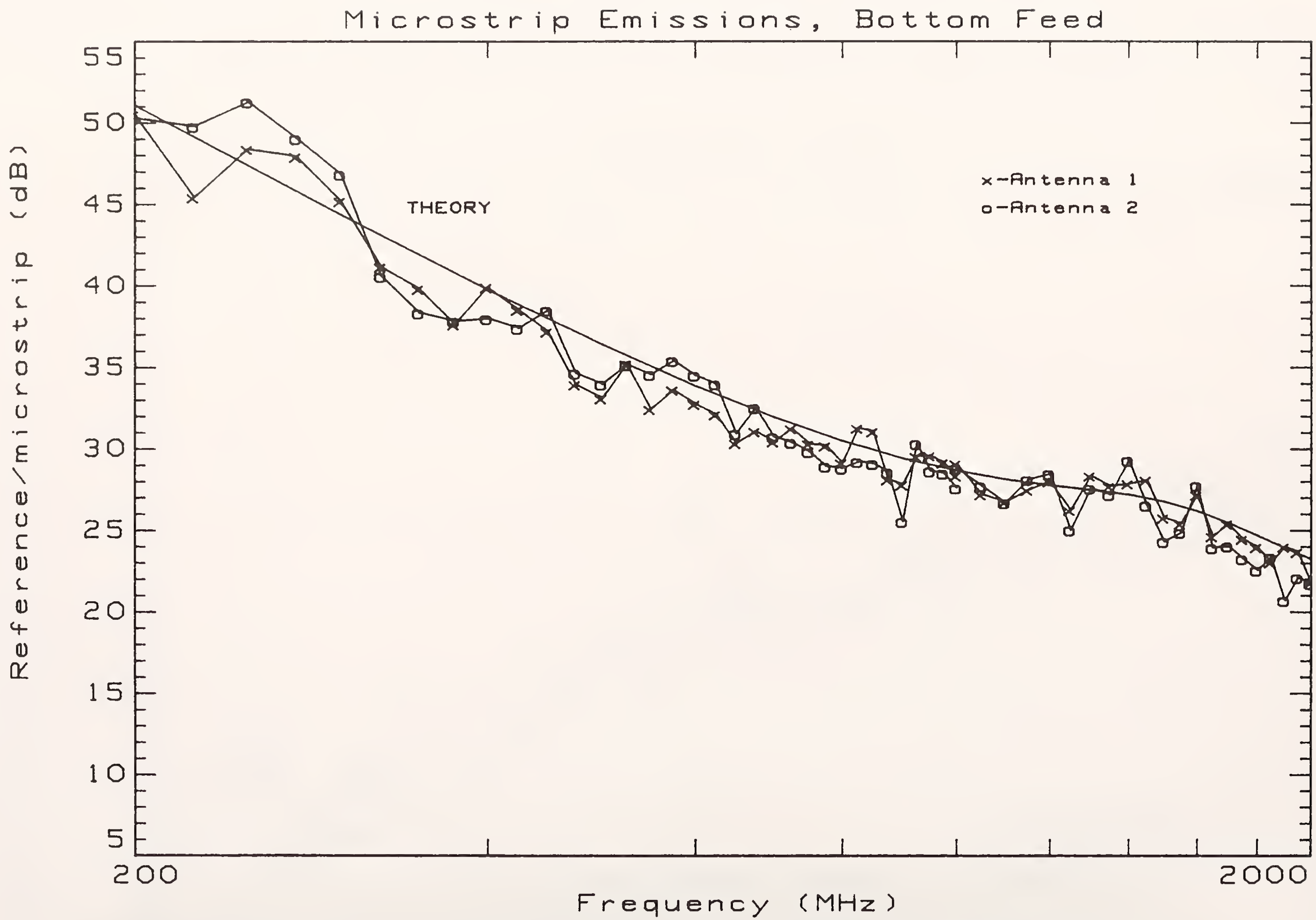

Figure 9. Microstrip (bottom feed) emissions measurements for two different receiving antennas.

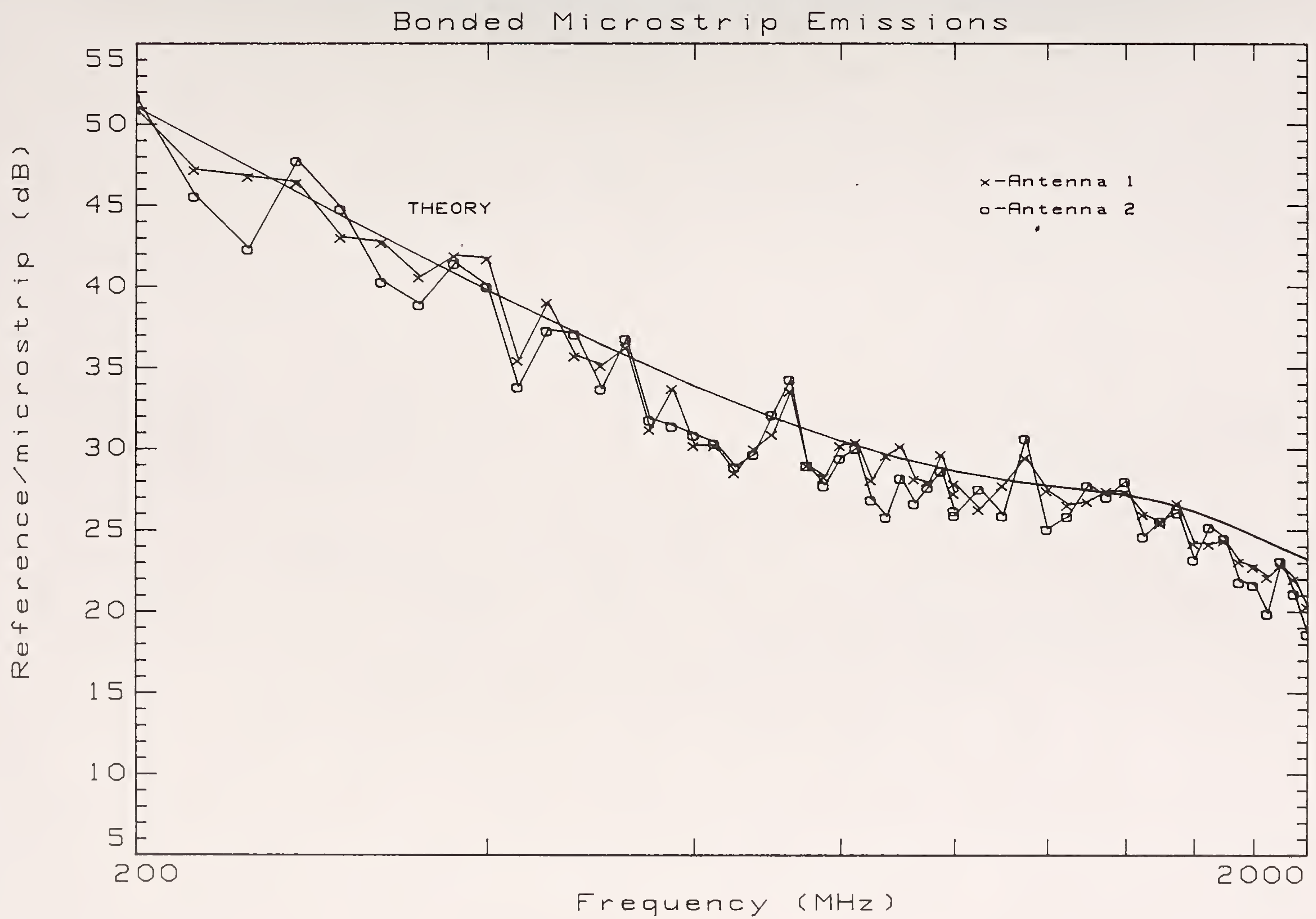

Figure 10. Microstrip (bonded to floor) emissions measurements for two different receiving antennas.

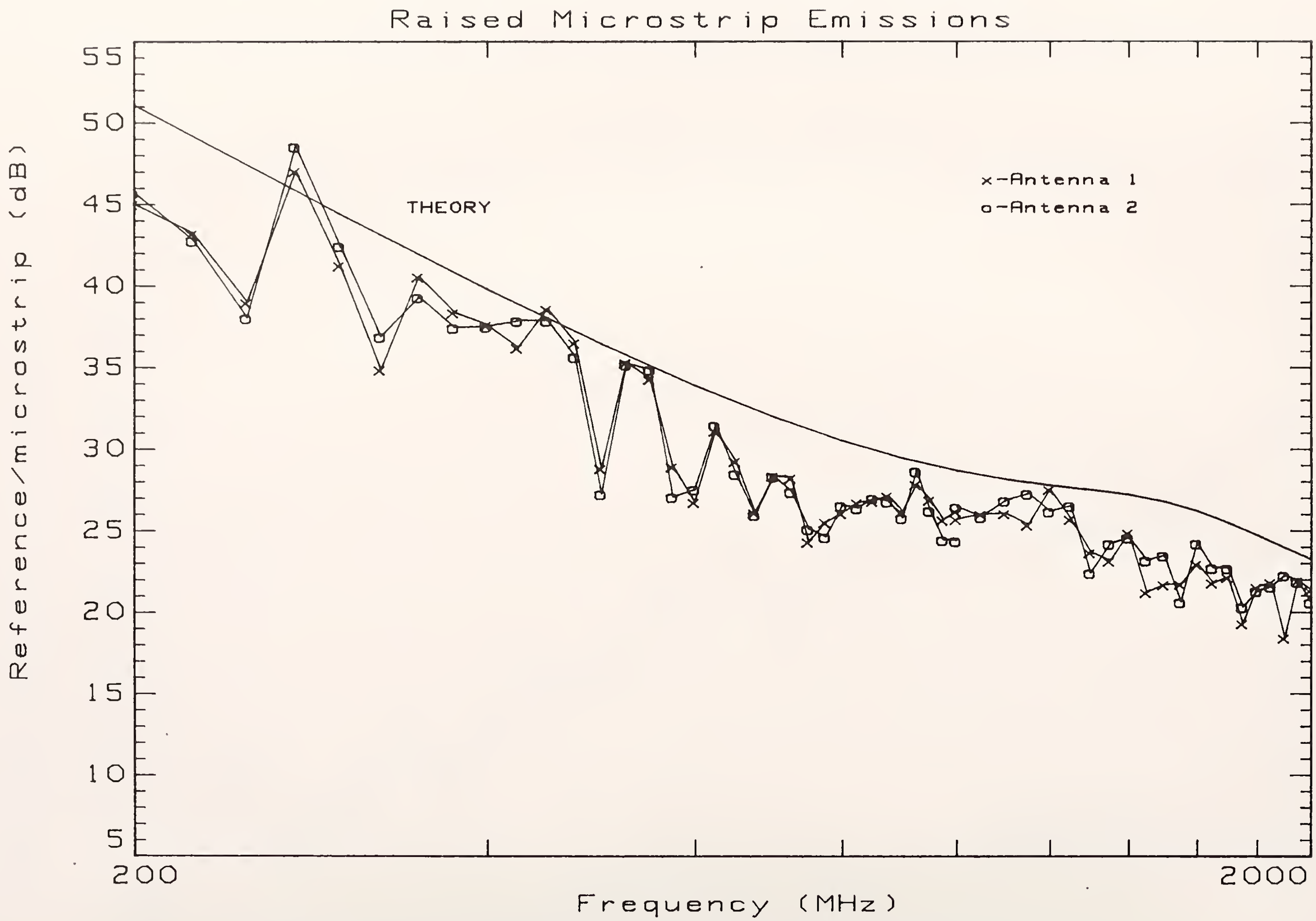

Figure 11. Microstrip (raised) emissions measurements for two different receiving antennas.

*U.S. GOVERNMENT PRINTING OFFICE:1995-673-018/00119

NIST Technical Publications

Periodical

Journal of Research of the National Institute of Standards and Technology—Reports NIST research and development in those disciplines of the physical and engineering sciences in which the Institute is active. These include physics, chemistry, engineering, mathematics, and computer sciences. Papers cover a broad range of subjects, with major emphasis on measurement methodology and the basic technology underlying standardization. Also included from time to time are survey articles on topics closely related to the Institute's technical and scientific programs. Issued six times a year.

Nonperiodicals

Monographs—Major contributions to the technical literature on various subjects related to the Institute's scientific and technical activities.

Handbooks—Recommended codes of engineering and industrial practice (including safety codes) developed in cooperation with interested industries, professional organizations, and regulatory bodies.

Special Publications—Include proceedings of conferences sponsored by NIST, NIST annual reports, and other special publications appropriate to this grouping such as wall charts, pocket cards, and bibliographies.

Applied Mathematics Series—Mathematical tables, manuals, and studies of special interest to physicists, engineers, chemists, biologists, mathematicians, computer programmers, and others engaged in scientific and technical work.

National Standard Reference Data Series—Provides quantitative data on the physical and chemical properties of materials, compiled from the world's literature and critically evaluated. Developed under a worldwide program coordinated by NIST under the authority of the National Standard Data Act (Public Law 90-396). NOTE: The Journal of Physical and Chemical Reference Data (JPCRD) is published bi-monthly for NIST by the American Chemical Society (ACS) and the American Institute of Physics (AIP). Subscriptions, reprints, and supplements are available from ACS, 1155 Sixteenth St., NW, Washington, DC 20056.

Building Science Series—Disseminates technical information developed at the Institute on building materials, components, systems, and whole structures. The series presents research results, test methods, and performance criteria related to the structural and environmental functions and the durability and safety characteristics of building elements and systems.

Technical Notes—Studies or reports which are complete in themselves but restrictive in their treatment of a subject. Analogous to monographs but not so comprehensive in scope or definitive in treatment of the subject area. Often serve as a vehicle for final reports of work performed at NIST under the sponsorship of other government agencies.

Voluntary Product Standards—Developed under procedures published by the Department of Commerce in Part 10, Title 15, of the Code of Federal Regulations. The standards establish nationally recognized requirements for products, and provide all concerned interests with a basis for common understanding of the characteristics of the products. NIST administers this program in support of the efforts of private-sector standardizing organizations.

Consumer Information Series—Practical information, based on NIST research and experience, covering areas of interest to the consumer. Easily understandable language and illustrations provide useful background knowledge for shopping in today's technological marketplace.
Order the **above** *NIST publications from: Superintendent of Documents, Government Printing Office, Washington, DC 20402.*
Order the **following** *NIST publications—FIPS and NISTIRs—from the National Technical Information Service, Springfield, VA 22161.*

Federal Information Processing Standards Publications (FIPS PUB)—Publications in this series collectively constitute the Federal Information Processing Standards Register. The Register serves as the official source of information in the Federal Government regarding standards issued by NIST pursuant to the Federal Property and Administrative Services Act of 1949 as amended, Public Law 89-306 (79 Stat. 1127), and as implemented by Executive Order 11717 (38 FR 12315, dated May 11, 1973) and Part 6 of Title 15 CFR (Code of Federal Regulations).

NIST Interagency Reports (NISTIR)—A special series of interim or final reports on work performed by NIST for outside sponsors (both government and non-government). In general, initial distribution is handled by the sponsor; public distribution is by the National Technical Information Service, Springfield, VA 22161, in paper copy or microfiche form.

U.S. Department of Commerce
National Institute of Standards and Technology
325 Broadway
Boulder, Colorado 80303-3328